JOURNAL OF THE CIVIL ENGINEERING FORUM

Journal of the Civil Engineering Forum, January 20XX, X(X): xx-xx
DOI 10.22146/jcef.XXXXX
Available Online at http: https://jurnal.ugm.ac.id/jcef/issue/archive

Behaviour of Precast Concrete Beam-to-Column Connection with SHS Hidden Corbel Subjected to Monotonic Load

Jen Hua Ling[1,*], Jee Hock Lim[2], Ahmad Baharuddin Abd. Rahman [3]
[1] School of Engineering and Technology, University College of Technology Sarawak, 96000 Sibu, Sarawak, MALAYSIA
[2] Lee Kong Chian Faculty of Engineering & Science, Department of Civil Engineering, Universiti Tunku Abdul Rahman 43000 Selangor, MALAYSIA
[3] School of Civil Engineering, Universiti Teknologi Malaysia, 81310 Skudai, Johor Darul Ta'zim, MALAYSIA
[*]Corresponding authors: lingjenhua@ucts.edu.my

SUBMITTED 7 January 2021 **REVISED** 29 January 2021 **ACCEPTED** 4 February 2021

ABSTRACT Beam-to-column connection is the most critical part of a precast concrete (PC) structure as it governs the integrity of the entire structure. For that, its characteristics need to be determined for safe applications in the construction industry. In this study, a beam-to-column connection with square hollow section (SHS) hidden corbel was developed. A full-scale test was conducted on eleven T-subframe specimens with various configurations to investigate the behaviour of the connection under an incremental static load. The behaviour of the connection was evaluated in terms of the moment-rotation response and the mechanical properties were obtained by using the beam-line method. The parametric response, the load resisting mechanism and the feasibility of the connection for PC structures were studied and discussed. Due to extensive usage of steel elements, the PC connection gave a higher ultimate strength than the reinforced concrete (RC) connection. Its moment resistance was largely contributed to by the hidden corbel embedded in the beam and column, which increased with the increase of the embedded length in the column and beam. The grout infill prevented the lateral deformation of the hidden corbel and thus strengthened the connection. Due to the low bending resistance of the steel endplate, the PC connection possessed a low stiffness, which led to a larger rotation deformation than the RC connection, and thus the design strength was low. This could be overcome by modifying the shape of the endplate for a higher second moment of inertia in resisting bending. The PC connection was classified as semi-rigid and partial-strength. Only specimen PC-3 was considered feasible for PC structures.

KEYWORDS Beam-to-column connection; precast; hidden corbel.

1 INTRODUCTION

Precast concrete (PC) structure is one of the construction methods popularly used in Malaysia. The building elements are prefabricated in factories under controlled environments with good quality assurance before being transported to construction sites for installation. This allows PC structures to be quickly erected with less consumption of energy and labour, and low risk of occupational safety and health (Zheng et al., 2018, Lu et al., 2019, Lin and Zhao, 2020).

The joint between the building elements is normally the weakest part of a PC structure (Choi et al., 2013). It governs the behaviour and integrity of the entire structure. The beam-to-column connection in PC structure connects the beams and columns. It is designed to have the ability to transfer loads from a member to another, such as shear, moment, axial, torsion, etc. The connection must be reliable, for structural stability, and preferably easy-to-install, for speedy construction.

For a wide variety of designs, the characteristics of connections are unique. It is thus important to acquire the behaviour of a connection for design purposes. Although PC elements are made of concrete, the connections demonstrate the characteristics of steel joints. This is due to the extensive usage of steel components in the connection to transfer loads and to facilitate installations.

For low deformability of concrete, the PC connection normally fails due to excessive cracking before the failure of the steel elements. Thus, determining the properties of the connection purely based on the steel components is likely overestimating the performance of the connection. For that, the beam-line method is normally used to determine the properties of PC connection (Elliott, 2002). These properties can then be used to classify the connection following Eurocode 3 (BS EN 1993-1-8:2005).

The characteristics of a newly developed beam-to-column connection can be determined from the full-scale destructive test (Jaspart, 1996, Lim, 2014). In this study, a beam-to-column connection with a hidden corbel made of square hollow section (SHS) was developed for non-seismic applications. An experimental test was carried out to acquire the structural behaviour and to classify the connection. The parametric response and the load resisting mechanism of the connection were also studied. Then, the connection was evaluated for feasibility in PC structures.

2 METHODS

2.1 Specimen details

Eleven full-scale T-subframe specimens were fabricated and tested under incremental monotonic load. This included two control specimens (i.e. RC0 and PC0) and nine test specimens (i.e. PC1 to PC9), each of which comprised a square column and a rectangular beam, which were designed based on the common sizes and reinforcements used in the local construction industry (Figure 1 and Table 1). The load was applied on the beam at a 1375 mm distance from the column face.

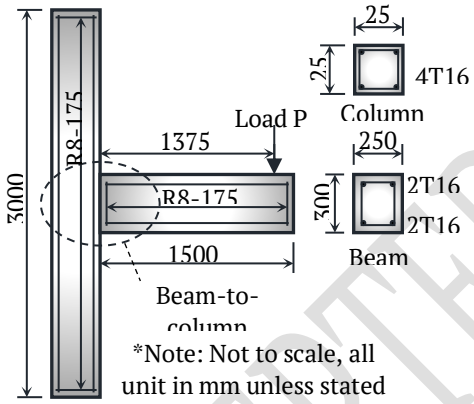

Figure 1. Details of specimen

Table 1. Dimension of specimen

	Beam	Column
Dimension	250 mm x 300 mm x 1500 mm	250 mm x 250 mm x 3000 mm
Reinforcements	Top and bottom bars, high yield strength steel bars 2T16 (f_{sy} = 460 N/mm^2)	High yield strength steel bars, 4T16 (f_{sy} = 460 N/mm^2)
Shear links	Mild steel bars, R8-175 (f_{sy} = 250 N/mm^2)	Mild steel bars, R8-175 (f_{sy} = 250 N/mm^2)
Concrete cover	41 mm	25 mm

The configuration of the specimens are described as follows:

a) Specimen RC0 represented a reinforced concrete (RC) joint (Figure 2(a)). The concrete was monolithically cast without any cold joint (Figure 3). The steel bars of the beam were embedded in the column at full anchorage length.

b) Specimen PC0 resembled a PC connection without SHS hidden corbel (Figure 2(b)). The steel bars in the beam were welded on a 20 mm thick steel endplate of grade S275. The endplate was then bolted to the column.
c) Specimens PC1 to PC9 were PC connections with SHS hidden corbel (Figure 2(c)). The design was identical to PC0 except there were two SHSs of different sizes embedded in the beam. During installation, the smaller SHS was slid and inserted into the column before the grout was poured in to fill the void (Figure 4).

The details of the connections are given in Table 2. The parameters studied included:
a) Effects of PC beam-to-column connection (RC0 vs PC0-9)
b) Effects of SHS hidden corbel (PC0 vs PC1-9)
c) Effects of size of hidden corbel (PC1-3)
d) Effects of embedded length of hidden corbel in column (PC3-5)
e) Effects of embedded length of hidden corbel in beam (PC3, 6 and 7)
f) Effects of grout in hidden corbel (PC3, 8 and 9)

The specimens were horizontally cast with grade 40 ready-mixed concrete in the laboratory. The design slump was 50 mm to 100 mm and the maximum aggregate size was 20 mm. The specimens were then cured in moist under wet jute sack for 7 days before installation on day 28.

During installation, high strength and non-shrink grout (Brand: *Sika-215*) of grade 70 was mixed into a pourable state with the mix proportion of 4 litres water per 25 kg grout power. The grout was poured into the hidden corbel through the grout inlet until an overflow of the grout was seen at the grout outlet. The compressive strength of the grout was closely monitored until the intended strength was achieved before the specimens were tested.

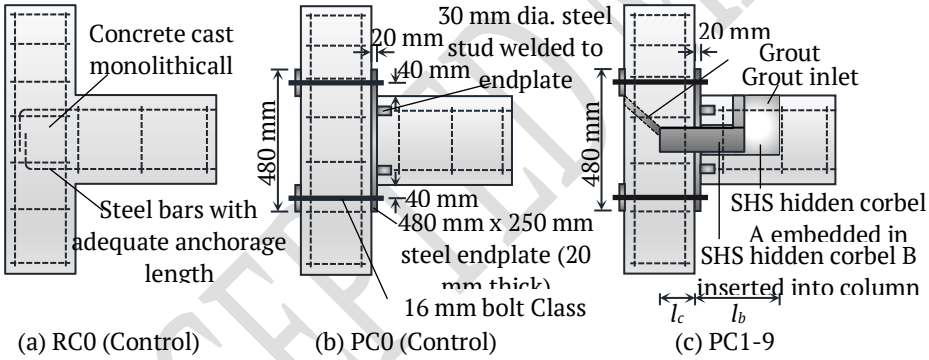

Figure 2. Design of specimens

(a) Reinforcement and formworks (b) Monolithic casting

Figure 3. Preparation of specimen RC0

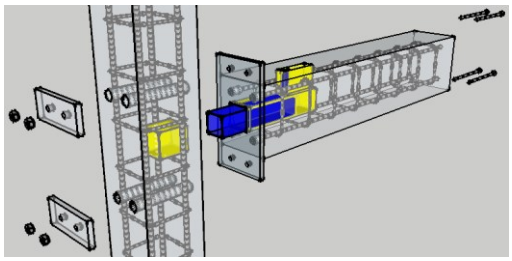

Figure 4. Installation of the connection

Table 2. Details of specimen

Specimen	Embedded length of hidden corbel in column, l_c (mm)	Embedded length of corbel in beam, l_b (mm)	SHS hidden corbel A size (mm)	SHS hidden corbel B size (mm)	Grout strength, $f_{u,g}$ (N/mm^2)
RC0	Monolithic reinforced concrete connection				
PC0	Precast concrete connection without SHS hidden corbel				
PC1	125	300	50.8	38.1	40
PC2	125	300	76.2	63.5	40
PC3	125	300	101.6	88.9	40
PC4	75	300	101.6	88.9	40
PC5	175	300	101.6	88.9	40
PC6	125	200	101.6	88.9	40
PC7	125	400	101.6	88.9	40
PC8	125	300	101.6	88.9	20
PC9	125	300	101.6	88.9	NIL

** Thickness of all SHSs was 3 mm*

2.2 Test setup

Steel frames were assembled in the laboratory to test the specimens. The support frame held the column in position while the load frame induced vertical load onto the beam (Figure 5(a) and Figure 5(b)). The column was restrained from horizontal displacement and moment rotation by inserting its ends into the grip buckets.

A hydraulic cylinder (Brand: *Enerpac*, capacity: 250 kN) was used to generate load acting on the beam at 1375 mm from the column face. A load cell (Brand: *TML*, capacity: 100 kN) was used to measure the load acting on the beam. Twelve linear variable displacement transducers (LVDT) (Brand: *TML*) and two inclinometers (Brand: *AccuStar*) were used to measure the displacement and rotation of the column and beam of the specimens (Figure 5(c)). Six LVDTs (H_1 to H_6) were used to measure the horizontal displacement of the column, while another six (V_1 to V_6) measured the vertical displacement of the beam. All the measuring devices were connected to a data logger (Brand: *TML*, 30 channels) for data acquisition.

Once completed setup, all readings were initialized to zero and the load was progressively increased at a rate of approximately 2.5 kN per reading taken. The load response and the crack propagation of the specimen were monitored throughout the test.

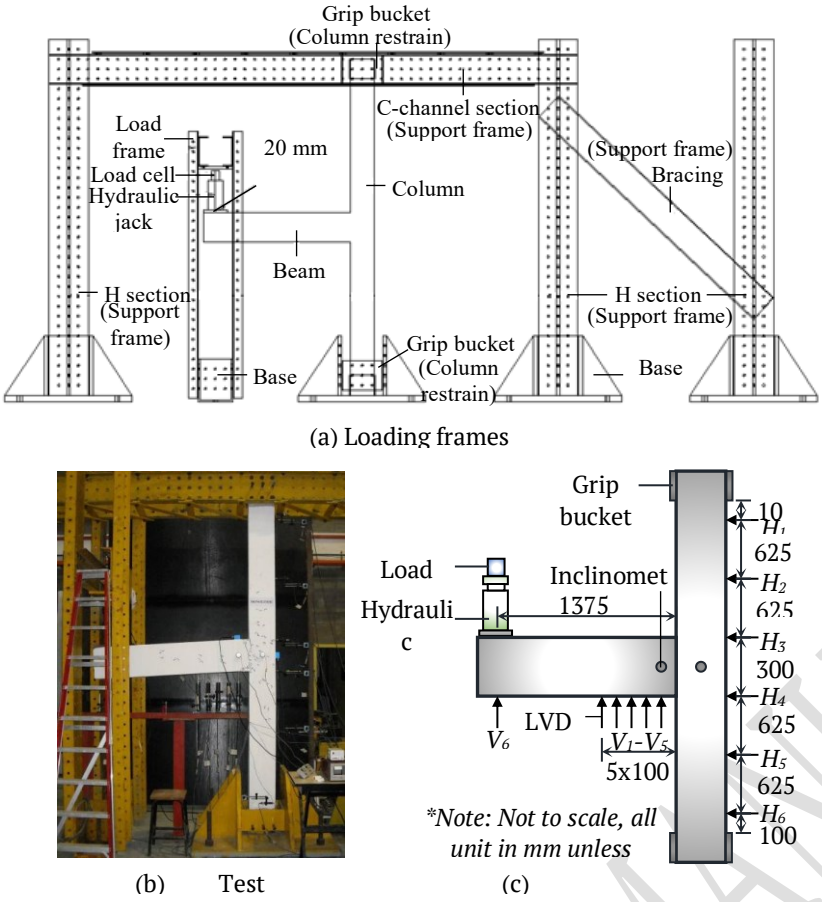

Figure 5. Test setup and instrumentation

3 RESULTS AND DISCUSSIONS

3.1 Material properties

The properties of materials used to fabricate the specimens are shown in Table 3 and Table 4. The compressive strength of concrete and grout were quite consistent and were close to their intended strengths of 40 N/mm^2. The yield strengths of the steel components were all higher than their nominal strengths of 460 N/mm^2 and 250 N/mm^2. Thus, the quality of materials was considered acceptable.

Table 3. Compressive strength of concrete and grout of the specimens

Specimens	Compressive strength of concrete, $f_{c,u}$ (N/mm^2)	Compressive strength of grout, $f_{g,u}$ (N/mm^2)
RC0	36.6	-
PC0	38.0	-
PC1	38.6	40.1
PC2	38.7	40.2
PC3	39.3	40.0
PC4	39.6	40.4
PC5	39.2	39.9
PC6	41.3	40.4
PC7	39.0	39.4
PC8	40.1	20.0
PC9	39.8	-

**Average values of 2 and 3 cube samples for concrete and grout respectively*

Table 4. Tensile strength of steel components of the specimens

Specimen	Yield Strength, f_y (N/mm^2)	Ultimate Strength, f_u (N/mm^2)	Young Modulus, E (kN/mm^2)	Strain Elongation (%)
Steel bars T16	525	611	210	14.47
Steel bars R8	450	506	234	14.85
20 mm thick steel endplate	303	384	229	19.67
38.1 mm SHS	321	358	202	7.64
50.8 mm SHS	278	338	202	11.99
63.5 mm SHS	319	399	202	9.39
76.2 mm SHS	303	351	204	9.79
88.9 mm SHS	326	375	200	11.63
101.6 mm SHS	346	389	202	9.70

**Average values of 3 steel samples*

3.2 Test results

The test results of the specimens are summarized in Table 5. The first crack load was determined when a crack was first detected on the surface of the specimen. The ultimate load was the highest load recorded throughout the test.

Table 5. Test results

Specimen	First Crack				Ultimate state			
	Load, P_{ic} (kN)	Vertical displacement, δ_{ic} (mm)	Beam rotation, $\phi_{b,ic}$ (°)	Column rotation, $\phi_{c,ic}$ (°)	Load, P_u (kN)	Vertical displacement, δ_u (mm)	Beam rotation, $\phi_{b,u}$ (°)	Column rotation, $\phi_{c,u}$ (°)
RC0	7.5	2.0	0.06	0.03	39.1	50.0	1.69	0.44
PC0	8.3	3.1	0.10	0.01	41.3	80.1	2.9	0.27
PC1	8.2	4.1	0.16	0.03	42.4	76.1	2.28	0.36
PC2	10.0	4.4	0.15	0.03	45.7	96.0	2.67	0.39
PC3	9.7	3.7	0.09	0.03	47.3	102.2	2.28	0.58
PC4	5.7	3.6	0.13	0.02	46.3	116.2	3.49	0.48
PC5	6.5	2.0	0.05	0.02	49.5	86.0	1.84	0.43
PC6	9.8	4.0	0.12	0.02	42.1	72.0	1.82	0.25
PC7	10.2	3.8	0.10	0.04	49.8	60.0	1.97	0.85
PC8	10.6	3.8	0.09	0.03	46.8	94.1	2.18	0.57
PC9	8.3	5.9	0.20	0.03	44.7	106.1	3.55	0.43

The data were then recomputed into the moment-rotation (M-ϕ) response using Equation (1) and Equation (2), as given in Table 6 and Figure 6.

$$M_i = P_i L \quad (1)$$

where M_i is the moment acting on the connection at different load levels (kNm), P_i is the load acting on the beam (kN), and L is the distance of the point load from the connection face (m).

$$\phi_i = \phi_{b,i} - \phi_{c,i} \quad (2)$$

where $\phi_{b,i}$ and $\phi_{c,i}$ are the moment rotation of the beam and column respectively (milli-rad).

Table 6. Moment and rotation of the specimen

Specimen	First crack			Ultimate state		
	Moment, M_{ic} (kNm)	Rotation, ϕ_{ic} (10^{-3} rad)	Stiffness, S_{ic} (kNm/10^{-3} rad)	Moment, M_u (kNm)	Rotation, ϕ_u (10^{-3} rad)	Stiffness, S_u (kNm/10^{-3} rad)
Equation	(1)	(2)	(3)	(1)	(2)	(3)
RC0	10.3	0.5	20.6	53.8	21.8	2.5
PC0	11.4	1.6	7.1	56.8	45.9	1.2
PC1	11.3	2.3	4.9	58.3	33.5	1.7
PC2	13.8	2.1	6.6	62.8	39.8	1.6
PC3	13.3	0.9	14.8	65.0	29.7	2.2
PC4	7.8	1.8	4.3	63.7	52.5	1.2
PC5	8.9	0.5	17.8	68.1	24.6	2.8
PC6	13.5	1.6	8.4	57.9	27.5	2.1
PC7	14.0	0.7	20.0	68.5	19.5	3.5
PC8	14.6	1.1	13.3	64.4	28.1	2.3
PC9	11.4	2.8	4.1	61.5	54.5	1.1

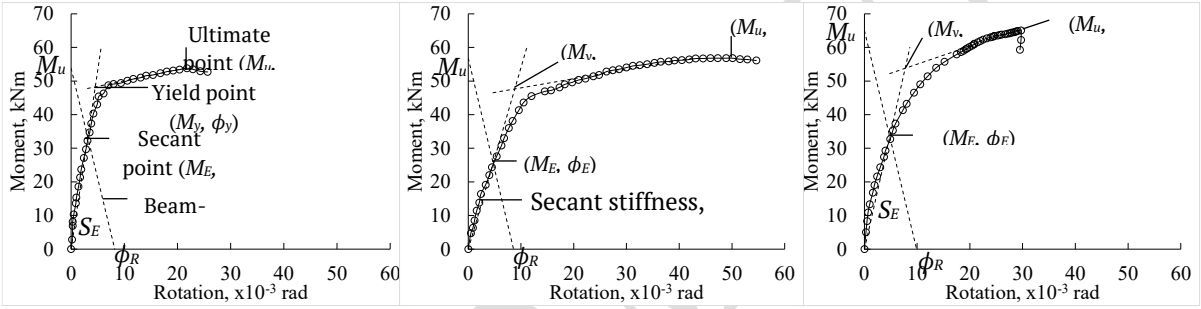

(a) Specimen RC0 (b) Specimen PC0 (c) Specimen PC3

Figure 6. Determining the properties of connection using beam-line method

The beam-line method proposed by Elliott (2002) was used to determine the properties of the specimens. The secant point (M_E, ϕ_E) was determined based on the characteristics of perfectly rigid and pinned connections. A rigid connection would have a moment capacity equivalent to the fixed-end moment of the beam it connects (Equation 3), and the rotation of a pinned connection would be governed by the rotational limit of an RC beam (Equation 4).

$$M_R = \frac{wL_b^2}{12} \quad (3)$$

$$\phi_R = \frac{wL_b^3}{24EI_b} \quad (4)$$

where M_R is the fixed-end moment of the continuous beam (kNm), ϕ_R is the allowable rotation of an RC beam (milli-rad), w is the uniform distributed load acting on the beam (kN/m), L_b is the beam span (m), E is the elastic modulus of concrete (kNm/milli-rad), and I_b is the second moment of inertia of the beam cross-section (m^4).

Assuming the ultimate moment capacity of the specimen, M_u was equivalent to the fixed-end moment of the beam, M_R, the allowable rotation of the connection, ϕ_R would be as given in Equation 5.

$$\phi_R = \frac{M_u L_b}{2EI_b} \quad (5)$$

where M_u is the ultimate moment capacity of the connection (kNm), L_b is the effective span of beam (m), which was assumed as 6 m (typical beam span), E is the elastic modulus of the beam (kN/m^2), which was taken as 35 GPa for concrete of grade 40 (BS-EN 1992-1-1:2004), and I_b is the second moment of inertia of the beam (m^4).

The beam-line intercepted the M-ϕ curve at the secant point (M_E, ϕ_E) and the gradient of the line connecting the secant point with the Origin was considered the secant stiffness, S_E (Equation 6).

$$S_E = \frac{M_E}{\phi_E} \quad (6)$$

The secant stiffness line was then extended to intercept with a best-fit straight line of the M-ϕ curve at the ultimate state to find the yield point (P_y, ϕ_y) (Figure 6). The properties of the connection determined by using the Beam-Line Method are summarized in Table 7.

The first crack moment, M_{ic}, was found about 1/5 of the ultimate moment, M_u (refer to the ratio M_{ic}/M_u in Table 8). Before the first crack, the connection would be in its best condition having the highest degree of stiffness.

The secant moment, M_E can be conservatively considered as the design strength of the connection, M_d (Lim, 2014). It was about 2 to 3 times the first crack moment, M_{ic} and 29% to 61% of the ultimate moment, M_u depending on the secant stiffness (Table 8). The design moments, M_d of the PC connections were generally lower compared with their ultimate moments, M_u. This led to a sizeable unutilized strength of the connection between M_u and M_d. In the case that M_u and ϕ_R are the same, the unutilized strength of the connection can be reduced with the increase of its stiffness, as demonstrated in Figure 7.

Table 7. Test results

	Rotation limit, ϕ_R (10^{-3} Rad)	Secant moment, M_E (kNm)	Secant rotation, ϕ_E (10^{-3} rad)	Secant stiffness, S_E (kNm/10^{-3} rad)	Yield moment, M_y (kNm)	Yield rotation, ϕ_y (10^{-3} rad)
Equation	(5)			(6)		
RC0	8.2	32.9	3.1	10.6	47.8	4.5
PC0	8.6	25.4	4.7	5.4	47.6	8.8
PC1	8.9	23.3	5.4	4.3	51.8	12.0
PC2	9.6	28.2	5.3	5.3	49.0	9.2
PC3	9.9	33.4	4.8	7.0	53.6	7.7
PC4	9.7	18.3	6.9	2.7	42.4	16.0
PC5	10.4	34.7	5.1	6.8	54.4	8.0
PC6	8.8	27.4	4.7	5.8	51.3	8.8
PC7	10.4	35.1	5.0	7.0	55.5	7.9
PC8	9.8	33.5	4.7	7.1	52.0	7.3
PC9	9.4	20.5	6.2	3.3	48.9	14.8

Table 8. Performance ratio

Specimen	M_{ic}/M_E	M_{ic}/M_y	M_{ic}/M_u	M_E/M_u	M_y/M_u	ϕ_E/ϕ_R	ϕ_y/ϕ_R	ϕ_u/ϕ_R	ϕ_u/ϕ_y
RC0	0.31	0.22	0.19	0.61	0.89	0.38	0.55	2.7	4.8
PC0	0.45	0.24	0.20	0.45	0.84	0.55	1.02	5.3	5.2
PC1	0.48	0.22	0.19	0.40	0.89	0.61	1.35	3.8	2.8
PC2	0.49	0.28	0.22	0.45	0.78	0.55	0.96	4.1	4.3
PC3	0.40	0.25	0.20	0.51	0.82	0.48	0.78	3.0	3.9

PC4	0.43	0.18	0.12	0.29	0.67	0.71	1.65	5.4	3.3
PC5	0.26	0.16	0.13	0.51	0.80	0.49	0.77	2.4	3.1
PC6	0.49	0.26	0.23	0.47	0.89	0.53	1.00	3.1	3.1
PC7	0.40	0.25	0.20	0.51	0.81	0.48	0.76	1.9	2.5
PC8	0.44	0.28	0.23	0.52	0.81	0.48	0.74	2.9	3.8
PC9	0.56	0.23	0.19	0.33	0.80	0.66	1.57	5.8	3.7

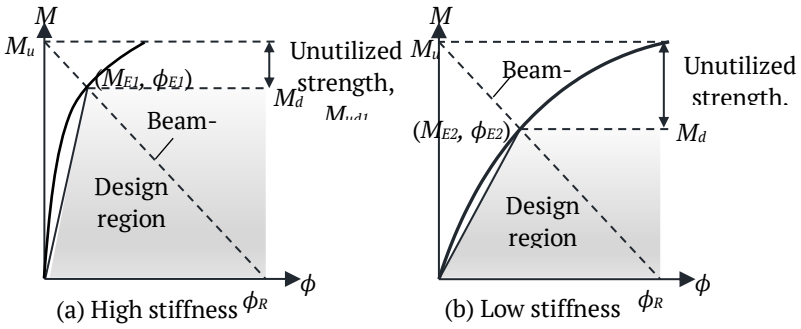

Figure 7. Effect of connection stiffness on the design strength

The yield point was an imaginary point when significant damage to the connection was expected. It was not considered as the design load because (a) it fell above the M-ϕ curve, which was not achievable by the connection in reality, (b) it underestimated the instantaneous rotation of the connection under loads, and (c) its rotation sometime exceeded the rotation limit of the beam ($\phi_y/\phi_R \geqslant 1.0$, Table 8).

3.3 Classification of connection

Adopting the principles by Eurocode 3 (BS EN 1993-1-8:2005), a PC connection can be classified by its stiffness and strength (Table 9).

Table 9. Classifications of connection based on stiffness and strength

Classification	Stiffness	Requirement
Stiffness (kNm/10^{-3} rad)	Pinned	$S_E \leq \frac{0.5EI_b}{L_b}$
	Semi-rigid	$\frac{0.5EI_b}{L_b} < S_E < \frac{k_bEI_b}{L_b}$
	Rigid	$S_E \geq \frac{k_bEI_b}{L_b}$
Strength (kNm)	Pinned	$M_d \leq 0.25M_{Rd}$
	Partial strength	$0.25M_{Rd} \leq M_d \leq M_{Rd}$
	Full strength	$M_d \geq M_{Rd}$

E is the modulus of elasticity of concrete (kN/m^2), I_b is the second moment of inertia (m^4), L_b is the beam span (m), k_b is equal to 8 and 25 for the braced and unbraced system respectively, M_d is the designed strength of the connection (kNm), M_{Rd} is the moment strength of the members (kNm).

The moment strength of the member, M_{Rd} was considered the smaller of the column, $M_{Rd,c}$ and the beam, $M_{Rd,b}$ (Equation 7), which can be determined from Equation 8 as the moment strength of an RC member.

$$M_{Rd} = \min\left(M_{Rd,c}, M_{Rd,b}\right) \quad (7)$$

$$M = \frac{f_{yk} z A_s}{\gamma_c} \quad (8)$$

where f_{yk} is the specified yield strength of the reinforcement bars, 500 N/mm^2; γ_c is the partial factor of safety of steel, 1.15; A_s is the cross-sectional area of the bar, 402 mm^2 for 2T16; and z is the lever arm of the stress block diagram (mm), which was assumed as 0.95d.

In general, the connection was considered semi-rigid and partial strength, as analysed in Table 10.

Table 10. Classification of the connection by stiffness

Classification	Stiffness					Strength		
Specimen	Pinned (kNm/10^{-3} rad)	Braced frame (kNm/10^{-3} rad)	Unbraced frame (kNm/10^{-3} rad)	Secant stiffness, S_E (kNm/10^{-3} rad)	Class	Design moment, M_d (kNm)	M_d/M_{Rd}	Class
PC0	1.6	26.3	82.0	5.4	S	25.4	0.73	P
PC1	1.6	26.3	82.0	4.3	S	23.3	0.67	P
PC2	1.6	26.3	82.0	5.3	S	28.2	0.81	P
PC3	1.6	26.3	82.0	7.0	S	33.4	0.96	P
PC4	1.6	26.3	82.0	2.7	S	18.3	0.53	P
PC5	1.6	26.3	82.0	6.8	S	34.7	1.00	F
PC6	1.6	26.3	82.0	5.8	S	27.4	0.79	P
PC7	1.6	26.3	82.0	7.0	S	35.1	1.01	F
PC8	1.6	26.3	82.0	7.1	S	33.5	0.97	P
PC9	1.6	26.3	82.0	3.3	S	20.5	0.59	P

*[1]E_b = 35000000 kN/m^2, I_b = 0.000562500000 m^4, L_b = 6 m; [2]Classification: R – Rigid, S – Semi-rigid, P – Pinned; [3]$M_{Rd,b}$ = 40.4 kNm, $M_{Rd,c}$ = 34.7 kNm, M_{Rd} = 34.7 kNm (Equation 7); [4]F – Full-strength ($M_d/M_{Rd} \geqslant 1.0$), P – Partial-strength ($0.25 < M_d/M_{Rd} < 1.0$), Pn – Pinned ($M_d/M_{Rd} \leqslant 0.25$)

3.4 Parametric response

The PC connection generally possessed a lower degree of stiffness than the RC connection. This was attributed to (a) the relative movements of the cold joints between the components of the connection and (b) the poor bending resistance of the steel endplate, both of which led to a larger instantaneous rotational deformation under the load.

Nevertheless, the PC connection gave a higher ultimate moment capacity, M_u than the RC connection due to (a) the extensive usage of the steel components and (b) the enhancement of the SHS hidden corbel. The PC connection without hidden corbel, PC0 had 5.6% higher M_u than the RC connection, RC0. As for those with hidden corbel (PC1 to PC9), M_u was 7.6% to 27.3% higher than RC0. Both the steel endplate and hidden corbel provided bending resistance to resist the load (Figure 8).

The ultimate moment, M_u of the connection increased as the embedded length of SHS hidden corbel in the column and beam increased. When the embedded length in the column increased from 75 mm to 150 mm, M_u increased 6.9%, and as the embedded length in the beam increased from 200 mm to 300 mm, M_u increased 18.3%. The longer embedded length provided a larger bearing area for the hidden corbel to effectively transfer stresses from the beam to the column.

The grout in the hidden corbel increased the ultimate moment of the connection. The connection with 20 N/mm^2 grout in the hidden corbel (PC8) gave a 4.7% higher M_u than the connection without the grout (PC9). However, as the grout strength increased from 20 N/mm^2 to 40 N/mm^2, M_u only increased by 0.9% (PC3 and PC8). The grout itself was weak in flexural bending. Its main function was to prevent the SHS hidden corbel from undergoing lateral deformation that affected the bending resistance of the connection.

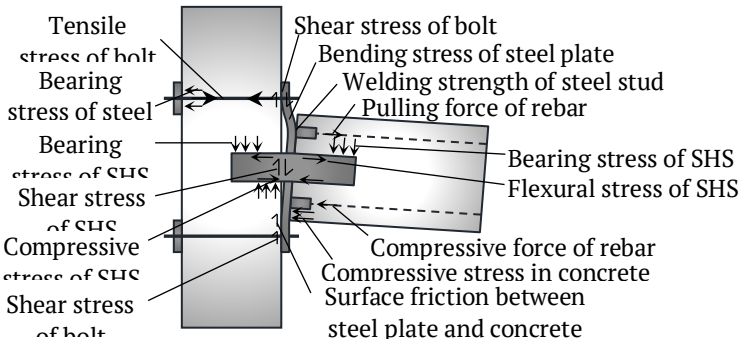

Figure 8. Load resisting mechanism of the connection

3.5 Failure mode

Table 11 outlines the failure mode of the specimens (Figure 9). In general, the load vertically displaced the free end of the beam, which subsequently led to the rotational deformation at the connection. The first crack occurred at the cold joint between the PC beam and the steel endplate. Then, cracks developed on the upper surface of the beam as the flexural crack. The cracks later headed toward the compressive region of the connection and eventually became the diagonal and peripheral cracks. The diagonal crack passed through the SHS hidden corbel while the peripheral crack bypassed it (Figure 9). Many specimens endured spalling at the tension region of the beam and some experienced crushing at the compressive region. The steel endplate bent considerably, which subsequently caused the dislocation of the steel stud welded to it and led to spalling of concrete.

Table 11. Failure modes of the specimens

Specimen	Beam					Joint		Column
	Crushing	Spalling	Diagonal crack	Peripheral crack	Flexural crack	Bended endplate	Vertical tearing crack	Diagonal tensile crack
RC0					L		H	L
PC0	H	L			L	H		
PC1	L	H	M			H		L
PC2		M	H			H		
PC3		M	H	M		H		L
PC4	H	H		H		H		L
PC5				H		M		M
PC6	H	M	H			M		M
PC7	H	L		H		M		M
PC8	M	M	H	L		M		H
PC9		H		M		H		L

*Severity rating based on visual observation: H – high, M – moderate, L – Low

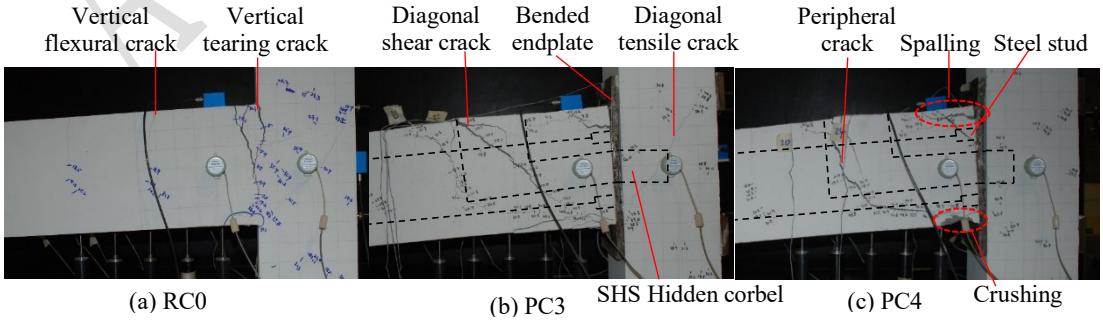

Figure 9. The typical failure mode of the connection

The responses of the connection components under load are outlined as follows: (refer to Figure 8)

a) The beam rotation generated bearing stress acting on SHS hidden corbel and created flexural load acting on it.
b) The pulling force of the top reinforcement bar generated bending stress in the steel endplate and tensile stress in the bolts.
c) The rotational movement of the beam triggered the compressive stress in the bottom reinforcement bars and the concrete. This subsequently led to frictional resistance between the steel endplate and the concrete.
d) The shear resistance of the bolts and the SHS hidden corbel resisted the vertical load preventing the beam from displacing vertically.

Based on the load resisting mechanism, the load capacity of the connection would be governed by (a) the tensile strength of the bolt, (b) the bending strength of the endplate, (c) the bending strength of the SHS, (d) the welding strength of the steel stud on the endplate, (e) the pullout strength between the top reinforcement bar and the steel stud and (f) the crushing strength of the concrete at the compressive region, whichever was weaker. In the case that the connection was stronger than the beam or column, the load capacity would be governed by the RC member.

The PC connections were generally stronger than the beam, as proven by the severe diagonal and peripheral cracks on the beam. Hence, specimens PC0 to PC9 generally gave a higher ultimate moment, M_u than RC0. However, the significant bending deformation of the steel endplate had caused the connection to experience large rotational deformation with low stiffness, which subsequently led to a low design strength of the connection over the ultimate load. To increase the design strength, the effective second moment of inertia of the steel endplate in resisting the bending deformation could be increased, as illustrated in Figure 10.

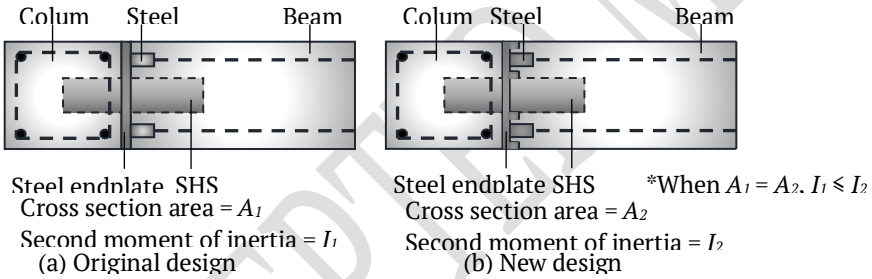

Figure 10. Comparison of the second moment of inertia of the steel endplate

4 FEASIBILITY EVALUATION

The feasibility of the PC connection was evaluated based on the following assessment criteria:

a) C1: The moment strength of the PC connection should be comparable to the RC connection. Thus, both the ultimate strength ratio, $R_{m,u}$ and the design strength ratio, $R_{m,d}$ should be at least 1.0.
   i. $R_{m,u} = \frac{M_{u,i}}{M_{u,c}} \geq 1.0$ (9)
   where $M_{u,i}$ and $M_{u,c}$ are the ultimate moment of PC and RC connections respectively (kNm).
   ii. $R_{m,d} = \frac{M_{d,i}}{M_{d,c}} \geq 1.0$ (10)
   where $M_{d,i}$ and $M_{d,c}$ are the design moment of PC and RC connections respectively (kNm).
b) C2: The connection should be ductile for survival purposes. Thus, the ductility ratio, R_{dc}, should be at least 4.0 for the low-moderate seismic region (Soudki, 1994, Ling et al., 2017).
   $R_{dc} = \frac{\phi_u}{\phi_d} \geq 4.0$ (11)

where ϕ_u is the rotation of connection at the ultimate state (milli-rad) and ϕ_d is the designed rotation of connection beam (milli-rad)

c) C3: The connection should not fail earlier than the beam. Therefore, the ultimate rotation of the connection should be greater than the allowable rotation of the beam, presumably at least 3 times more.

$$R_r = \frac{\phi_u}{\phi_R} \geq 3.0 \quad (12)$$

d) C4: The design moment should not be too low compared with the ultimate moment so that the connection is more efficiently utilized. The design ratio, R_d, should be at least 0.5.

$$R_d = \frac{M_d}{M_u} \geq 0.5 \quad (13)$$

where M_d is the design moment of connection (kNm), M_u is the ultimate moment of connection (kNm)

e) C5: For the complexity in predicting the beam rotation, as the SHS hidden corbel of the connection may have altered (i.e. shortened) the effective length of the beam in computing ϕ_R, some allowance of beam rotation may be required to ensure the rotation limit of the beam is not exceeded. The designed rotation is preferably below 50% of the allowable rotation.

$$R_a = \frac{\phi_d}{\phi_R} \leq 0.5 \quad (14)$$

where ϕ_d is the design rotation of connection (milli-rad) and ϕ_R is the rotation limit of connection (milli-rad)

Table 12 demonstrates the feasibility evaluation of the connection. The connections were considered feasible when all the assessment criteria were fulfilled.

Based on the evaluation, specimen PC3 was found feasible for PC structure. It may not have the largest moment capacity but performed relatively well in various aspects. The second best option would be PC8, which had scored five out of six criteria. The non-compliance in criteria C3 (R_r = 2.9) was rather close to the requirement of 3.0.

The main difference between specimens PC3 and PC8 was the grout strength of 40 N/mm^2 and 20 N/mm^2, respectively. This reveals the need of having the SHS hidden corbel filled with grout, but not necessarily high strength.

Table 12. Classification of connection by the strength

Criteria	C1(i)	C1(ii)	C2	C3	C4	C5	Score*[1]	Feasible*[2]
Ratio	$R_{m,u}$	$R_{m,d}$	R_{dc}	R_r	R_d	R_a		
Equation	(9)	(10)	(11)	(12)	(13)	(14)		
Requirement	⩾1.0	⩾1.0	⩾4.0	⩾3.0	⩾0.5	⩽0.5		
PC0	1.06	0.77	9.8	5.3	0.45	0.55	3/6	N
PC1	1.08	0.71	6.2	3.8	0.40	0.61	3/6	N
PC2	1.17	0.86	7.5	4.1	0.45	0.55	3/6	N
PC3	1.21	1.02	6.2	3.0	0.51	0.48	6/6	Y
PC4	1.18	0.56	7.6	5.4	0.29	0.71	3/6	N
PC5	1.27	1.05	4.8	2.4	0.51	0.49	5/6	N
PC6	1.08	0.83	5.9	3.1	0.47	0.53	3/6	N
PC7	1.27	1.07	3.9	1.9	0.51	0.48	4/6	N
PC8	1.20	1.02	6.0	2.9	0.52	0.48	5/6	N
PC9	1.14	0.62	8.8	5.8	0.33	0.66	3/6	N

*[1]Score – number of criteria fulfilled / total number of criteria; [2]Y – Feasible, N – Not feasible

5 CONCLUSION

In this study, an experimental test was conducted on eleven full-scale T-subframe specimens to investigate the behaviour of precast concrete beam-to-column connection with SHS hidden corbel. The mechanical properties of the connections were determined based on the beam-line method, and the connections were classified following Eurocode 3. The connections were found semi-rigid and partial-strength.

Due to the steel components, the PC connection offered a 6% to 27% higher ultimate moment than the RC connection. However, due to low stiffness, the design strength of the PC connection was generally lower than the RC connection.

The SHS hidden corbel contributed to the moment resistance of the connection. Its embedded length in the column and the beam increased the moment strength of the connection. The grout infill was found essential to strengthen the hidden corbel, but the effects of the increasing grout strength on the connection were minimal.

Excessive bending deformation of the steel endplate was identified to be the root cause of low stiffness and design strength of the connection, which subsequently led to ineffective utilization of the moment capacity. The steel endplate could be modified to increase the second moment of inertia for higher efficiency of the connection design.

The feasibility of the connection was evaluated in various aspects, namely the strength, ductility, serviceability and design tolerance of a connection. The evaluation was done on basis of relative comparison among the test specimens. Specimen PC3 was found fulfilling all the evaluation criteria and thus was considered feasible.

DISCLAIMER

The authors declare no conflict of interest.

ACKNOWLEDGMENTS

This research was supported by the Research Grants of the Ministry of Higher Education, Vot 78013.

REFERENCES

BS-EN 1992-1-1:2004, 2004. Eurocode 2: Design of concrete structures - Part 1-1: General rules and rules for buildings.

BS EN 1993-1-8:2005, 2005. Eurocode 3: Design of steel structures - Part 1-8: Design of joints.

Choi, H. K., Choi, Y. C. & Choi, C. S., 2013. Development and Testing of Precast Concrete Beam-to-Column Connections. *Engineering Structures*, 56, pp 1820-1835.

Elliott, K. S., 2002. *Precast Concrete Structure*, Butterworth-Heinemann.

Jaspart, J. P., 1996. *Structural Connections: Experimental as Design Tool*. Seminar Structural Assessment: The Role of Large and Full Scale Testing. City University, London

Lim, J. H., 2014. *Experimental Behaviour of Exterior Hybrid Precast Concrete Beam-to-Column Connections Subjected to Monotonic Load*. PhD thesis, Universiti Teknologi Malaysia.

Lin, F. & Zhao, P., 2020. Behavior of Grouted Sleeve Splice for Steel Profile under Tensile Loadings. *Materials*, 13(9), 2037.

Ling, J. H., Abd. Rahman, A. B., Ibrahim, I. S. & Abdul Hamid, Z. 2017. An Experimental Study of Welded Bar Sleeve Wall Panel Connection under Tensile, Shear, and Flexural Loads. *International Journal of Concrete Structures and Materials*, 11, pp 525-540.

Lu, Z., Huang, J., Li, Y., Dai, S., Peng, Z., Liu, X. & Zhang, M., 2019. Mechanical Behaviour of Grouted Sleeve Splice under Uniaxial Tensile Loading. *Engineering Structures*, 186, pp 421-435.

Soudki, K. A., 1994. *Behaviour of Horizontal Connections for Precast Concrete Load-bearing Shear Wall Panels Subjected to reversed Cyclic Deformations*. PhD thesis, University of Manitoba.

Zheng, Y., Guo, Z., Guan, D. & Zhang, X., 2018. Parametric Study on a Novel Grouted Rolling Pipe Splice for Precast Concrete Construction. *Construction and Building Materials*, 166, pp 452-463.